Pramana – J. Phys. (2017) 89:30
DOI 10.1007/s12043-017-1423-y

Low-energy electron impact cross-sections and rate constants of NH_2

ANAND BHARADVAJA[1,*], SAVINDER KAUR[2] and K L BALUJA[3]

[1]Department of Physics, Bhaskaracharya College of Applied Sciences, University of Delhi, New Delhi 110 075, India
[2]Department of Physics, SGTB Khalsa College, University of Delhi, Delhi 110 007, India
[3]Formerly at: Department of Physics and Astrophysics, University of Delhi, Delhi 110 007, India
*Corresponding author. E-mail: anand.bharadvaja@bcas.du.ac.in

MS received 24 August 2016; revised 15 February 2017; accepted 22 February 2017; published online 24 July 2017

Abstract. This systematic study reports various electron impact cross-sections, rate constants and transport properties of NH_2 radical in the low-energy limit. The collision study is based on *R*-matrix formalism and involves the use of various scattering models employing different active spaces. Both electron excited inelastic cross-sections and resonances are found influenced by correlation and polarization effects. The non-relativistic molecular bremsstrahlung radiation cross-section for soft photons, binary encounter Bethe model-based ionization cross-sections and a few molecular properties of the target radical are also reported. The present calculations are found to be in agreement with the available results. This theoretical study provides a pathway to understand collision dynamics and generates data required in various fields of applied physics.

Keywords. *R*-matrix; cross-section; configuration interaction; resonance; rate constant; bremsstrahlung radiation; collision frequency.

PACS Nos 34.80.Bm; 34.80.Gs; 34.80.Ht

1. Introduction

The nitrogen-based radicals are important intermediate species in many chemical reactions. They contribute significantly to transformations in the atmosphere, living organisms, chemical synthesis, combustion and detonation amongst others [1]. The strength of any electron–molecule interaction is measured in terms of scattering cross-sections. The scattering cross-sections are of importance in industrial, astrophysical, atmospheric and biological processes [2], modelling of combustion phenomenon [3,4] etc. The $e^- - NH_2$ collision plays an important role in combustion [5], atmospheric chemistry of nitrogen containing compounds [6], thermal decomposition of hazardous species [7–9], plasma processing [10–12], formation and destruction of NO_x from nitrogen-containing compounds in fuels [13,14] etc. The NH_2 radical also known as amidogen is an important constituent in planetary and cometary atmosphere and has been the subject of several investigations [15–17]. It can be generated by either hydrogen abstraction or UV photolysis in laboratory [18] and atmosphere [19].

The physical and chemical properties of this radical are very well studied in terahertz range molecular spectroscopy [20,21]. Several theoretical studies are there to determine its structural properties [22–27]. However, limited information is available for the electron–NH_2 scattering. Brescansin *et al* [28] used Schwinger method to obtain elastic, differential, momentum transfer and rotationally summed cross-sections. Joshipura *et al* [29] used optical potential method to extract elastic and ionization cross-sections. Tarnovsky *et al* [30] and Deutsch *et al* [31] determined ionization cross-sections based on theoretical and experimental approach. We report the electron impact elastic, excitation cross-sections and rate constants using the UK *R*-matrix molecular codes (UKRMoL) [32]. Different scattering models are used to understand the effect of correlation-polarization on collision phenomenon. The differential and momentum transfer cross-sections are determined using POLYDCS code [33]. The non-relativistic molecular bremsstrahlung radiation cross-sections for soft photons, collision frequencies and ionization cross-sections based on binary encounter Bethe (BEB) model

are also reported. This comprehensive study would be useful in modelling plasma-induced processes, matter-radiation interaction and in various other fields of physics as there is a scarcity of collision data. It is emphasized that the comparison with the previous results is an important part of the present study to establish the quality of the present results.

1.1 *Method: R-matrix*

The *R*-matrix method is an *ab-initio* method based on variational principle. It was originally developed by Wigner to study nuclear reactions [34,35] and later used by Burke *et al* to study electron collision with atoms [36]. This method successfully describes electron scattering from molecules and ions [37,38]. In the *R*-matrix approach, the electron configuration space is split into inner and outer regions. The radius of the inner region is taken to be $12a_0$. It encloses the entire charge distribution of the target molecule and is centred on the centre of gravity of the molecule. At this radius, the amplitudes of the molecular orbitals are negligible (less than $10^{-5}a_0^{-3/2}$). The correlation and exchange effects are considered in the inner region. The target and continuum orbitals are represented by a set of Gaussian orbitals and are orthogonalized using Schmidt orthogonalization. The continuum molecular orbitals are then orthogonalized among themselves using symmetric or Löwdin orthogonalization to remove the linearly-dependent functions [39,40].

The wave function of the $N+1$ scattering system ($NH_2 + e^-$) in the inner region is represented by a configuration interaction (CI)-type basis expansion [41]:

$$\Psi_k^{N+1} = A\sum_i \phi_i^N(x_1,\ldots,x_N)\sum_j \xi_j(x_{N+1})a_{ijk} + \sum_m \chi_m(x_1,\ldots,x_N,x_{N+1})b_{mk}, \quad (1)$$

where A is an antisymmetrization operator, $x_i,\ldots,x_N$ are the spatial and spin coordinates of the Nth electron, ϕ_i^N is the wave function of the ith target state, ξ_j are the continuum orbitals of the scattering electron, k represents a particular *R*-matrix basis function. The variational coefficients a_{ijk} and b_{mk} are determined by matrix diagonalization. Unlike the bound orbital basis function, the continuum orbitals basis do not vanish on the boundary. The χ_m are L^2 functions constructed from the occupied and virtual molecular orbitals of the target and hold both the target and the projectile electrons. The L^2 configurations are of two types. A subset of these relaxes the enforced orthogonality between the target and the continuum orbitals. There are others that give rise to correlation configurations which arise when the scattering electron occupies an extra virtual orbital that compensates the truncated partial wave expansion to a certain degree. The L^2 functions are also responsible for electron correlation–polarization and resonance effects, and also ensure the completeness of the basis function when the continuum orbital basis are orthogonalized to the bound electron basis. The static exchange (SE) model in eq. (1) has a single Hartree–Fock ground state in the first sum. The second sum runs over the minimal number of configurations required to relax the orthogonality constraint between the target molecule orbitals and the functions to represent the configuration. In the SE model, polarization effects are neglected.

In the outer region, the scattering electron is identifiable; the exchange and electron–electron correlation effects are neglected. However, the long-range interactions between the scattering electron and the target are considered. A single-centre multipole expansion of the electron–molecule interaction potential is sufficient to describe the physical effects. This multipole expansion includes dipole and quadrupole moments. The radial behaviour of the electron in the outer region is described by the set of coupled differential equations which are solved by propagating the inner boundary radius from $12a_0$ to $50a_0$. Beyond $50a_0$, the radial functions are matched with asymptotic functions [42,43] to extract K and T matrices in order to obtain cross-sections. Also beyond $50a_0$, the electrons are free and are represented by Bessel functions. The calculations in *R*-matrix formalism are performed within the fixed-nuclei approximation.

1.2 *Target model*

NH_2 belongs to C_{2v} point-group symmetry having a ground-state electronic configuration $1a_1^2 2a_1^2 1b_2^2 3a_1^2 1b_1^1$ ($X\ ^2B_1$). The self-consistent field (SCF) procedure is used to generate the molecular orbitals. The two frozen electrons are placed in $1a_1$ orbital while the seven free electrons move in $2a_1$, $3a_1$, $1b_1$, $1b_2$ molecular orbitals and in virtual orbitals like $4a_1,\ldots,2b_1,2b_2\ldots$, and so on. The inclusion of electrons in virtual orbitals gives rise to different sets of active spaces like $(4a_1, 1b_1, 2b_2)$, $(5a_1, 2b_1, 3b_2)$, $(6a_1, 2b_1, 4b_2)$, $(8a_1, 2b_1, 4b_2)$ etc. The active space $(4a_1, 1b_1, 2b_2)$ implies that there are $1a_1\ldots4a_1, 1b_1, 1b_2\ldots2b_2$ molecular orbital electrons; free to move among themselves to form configuration state functions (CSFs). The double zeta plus polarization (DZP) Gaussian basis set [41] contracted to $(9,5,1)/(4,1)$ for N atom and for H atoms are used.

Table 1. Ground-state target parameters at experimental geometry [26] in 3-states CI model using different active spaces.

Parameters	(4, 1, 2)	(5, 2, 3)	(6, 2, 3)	(6, 2, 4)	(7, 2, 4)	(8, 2, 4)	(8, 2, 4, 1)
Energy (a.u.)	−55.584	−55.622	−55.634	−55.651	−55.669	−55.679	−55.689
Correlation energy (eV)	−0.38	−1.36	−1.66	−2.09	−2.61	−2.88	−3.14
CSFs	49–60	1496–1552	3430–3556	7112–7550	13742–14666	24924–27300	45144–46089

Table 2. Vertical excitation energy (eV) of low-lying excited states in 3-states CI model in different active spaces.

Symmetry	State electronic configuration	(4, 1, 2)	(5, 2, 3)	(6, 2, 3)	(6, 2, 4)	(7, 2, 4)	(8, 2, 4)	(8, 2, 4, 1)
$1\,^2A_1$	$1a_1^2 2a_1^2 1b_2^2 3a_1^1 1b_1^2$	2.44	2.33	2.29	2.27	2.267	2.262	2.259
$1\,^2B_2$	$1a_1^2 2a_1^2 1b_2^1 3a_1^2 1b_1^2$	7.27	6.97	6.92	6.90	6.89	6.88	6.86

Table 3. Comparison of target parameters obtained using 3-states CI model in (6, 2, 4) with other works.

Parameter	This work	Other works				
Dipole moment (a.u.)	0.803	0.68 [23]	0.803 [24]	0.716[a] [45]	0.803 [28]	–
Transition moment (a.u.)						
$X\,^2B_1 \rightarrow 1\,^2A_1$	0.268	0.26 [25]	0.263 [46]	0.314 [24]	–	–
Vertical excitation energy (eV)						
$X\,^2B_1 \rightarrow 1\,^2A_1$	2.27	2.07[a] [47]	2.20 [22]	2.16 [48]	2.26 [27]	2.199 [46]
$X\,^2B_1 \rightarrow 1\,^2B_2$	6.90	6.50 [22]	6.51 [27]	6.64 [48]	–	–
Vertical ionization energy (eV)	13.64	12.0[a] [49]	–	–	–	–
Quadrupole moments (a.u.)						
Q_{20}	0.96	–	–	–	–	–
Q_{22}	0.98	–	–	–	–	–

[a]Experimental value.

The ground-state target properties are studied in different active spaces at an equilibrium geometry of $R_{N-H} = 1.024$ Å and $\angle$H–N–H $= 103.4°$ [26].

The trial wave function of the scattering system (electron + target states) is expanded in terms of the ground and few low-lying excited states below the threshold level. This model, termed many-states CI model, includes $^2B_1$,$^2A_1$ and $^2B_2$ states in the trial wave function and is characterized by both open and closed channels. The index i in eq. (1) thus varies from 1 to 3. This 3-states CI model incorporates both the polarization and correlation effects, thereby correctly representing the electron–target molecular system. The accurate representation of target wave function is of paramount importance for the correct description of the scattering phenomenon. In the R-matrix formalism, we are constrained to use a single orbital basis set to represent all the target states. This results in the excitation thresholds which are slightly higher than the experimental values.

The first vertical ionization energy was determined from the singly occupied $1b_1$ molecular orbital using the restricted Hartree–Fock formalism [44]. The various target parameters obtained using 3-states CI model in different active spaces are summarized in tables 1, 2 and 3. These are in good agreement with their respective experimental and theoretical values as evident from table 3. The justification for referring to active space (6, 2, 4) in table 3 is given in the next section.

1.3 *Scattering model*

Of the several possible active spaces mentioned in the previous section, the R-matrix scattering calculations are confined to the active space (6, 2, 4) for the following reasons: (i) The excitation cross-sections are sensitive to threshold energies. The vertical excitation energies (table 3) of the lowest two states included in CI model were almost the same in the active spaces (6, 2, 4),

(7,2,4), (8,2,4) and (8,2,4,1). (ii) The effect of coupling on the scattering calculations was minimized by including higher orbitals up to +33.6 eV energy. The number of CSFs generated in various active spaces are mentioned in table 1.

The target radical has doublet spin multiplicity and hence, the scattering calculations are performed for singlet and triplet states in C_{2v} symmetry. The continuum orbitals up to g partial wave are represented by the Gaussian centred at the molecule centre of gravity [50] in scattering calculations.

The large dipole moment, 2.04 D, of NH_2 radical reflects its strong polar nature. A polar molecule in fixed-nuclei approximation shows a strong diverging nature at low energies and small scattering angles. A large number of partial waves are therefore, required to obtain converged cross-sections. The R-matrix cross-sections (σ^R) contain only finite number of partial waves ($l \leq 4$). The contribution arising from higher partial waves ($l > 4$) termed as Born correction can be calculated using the analytic Born cross-section. The Born correction in closed form as a function of energy E can be written as

$$\delta\sigma^B(E) = \sigma^B(E) - \sigma^B_{l\leq 4}(E). \quad (2)$$

This correction can be applied directly to the R-matrix cross-sections without the explicit inclusion of the rotational motion by a top-up procedure defined by the following equation:

$$\sigma(E) = \sigma^R(E) + \delta\sigma^B(E). \quad (3)$$

This approach was used while studying electron scattering from polar molecules like OClO [51] and Cl_2O [52].

Alternatively, the integral cross-sections can be obtained from differential cross-sections (DCS) by including rotational motion along with a very large number of partial waves. This approach overcomes the singularity arising in DCS at low energies in the forward direction. The POLYDCS [33] based on multipole extracted adiabatic nuclei (MEAN) method [53] is used to obtain the DCS. The methodology is explained in §2.4. It is pertinent to mention that the elastic cross-sections obtained using two different approaches, (a) R-matrix and (b) rotational DCS, yield the same results.

2. Results

2.1 *Elastic and inelastic cross-sections*

The collision of an electron with a molecule can either be elastic or inelastic. The elastic collision is an important mechanism to study the collision transport properties. In an inelastic collision, transfer of kinetic energy causes electronic, rotational or vibrational excitations, thus changing the internal energy of the molecule and the momentum between the colliding partners. The electronic excitation process is a key process in understanding the hydrogen plasmas. The Born-corrected R-matrix elastic cross-sections (ECS) computed using eq. (3) in 3-states CI model are plotted in figure 1. The large cross-sections in low-energy limit are due to the dominating effect of long-ranged dipole interaction. These Born-corrected R-matrix cross-sections are in good agreement with that of Brescansin *et al* [28] who used Schwinger method to solve the scattering equations. Their optical potential method included static, exchange and correlation–polarization effects. In 3-states CI model, only $1\,^2A_1$ is dipole coupled with the ground state. Due to this, there is an overlap of 1- and 3-states CI model cross-sections in figure 1. The inclusion of excited states in CI model allows us to obtain electron excited cross-sections within R-matrix formalism. These cross-sections are reported in figures 2 and 3.

Expectedly, the dipole-forbidden inelastic cross-sections in figure 3 are much smaller than the dipole-allowed inelastic cross-sections (figure 2). All inelastic

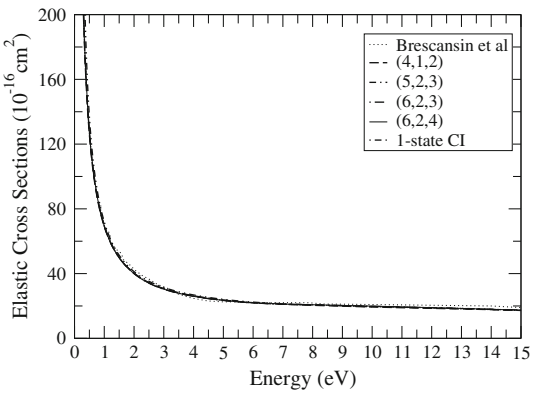

Figure 1. Elastic cross-sections.

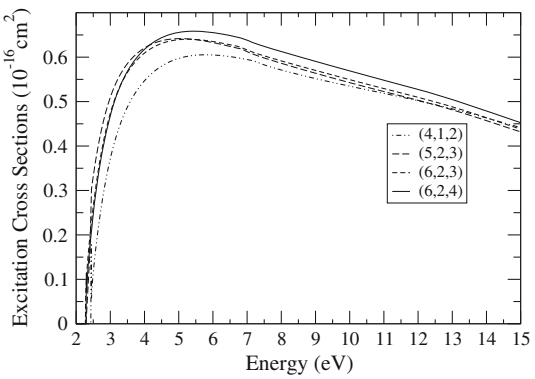

Figure 2. Excitation cross-sections for $X\,^2B_1 \rightarrow 1\,^2A_1$.

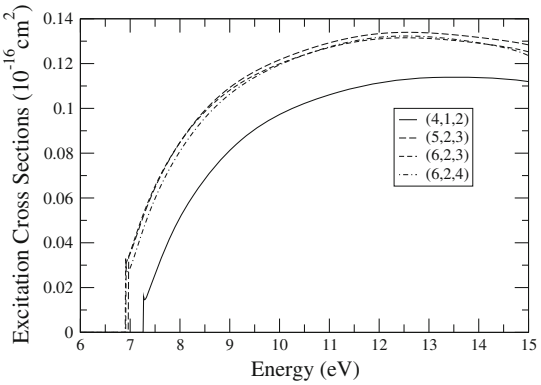

Figure 3. Excitation cross-sections for X $^2B_1 \rightarrow 1\,^2B_2$.

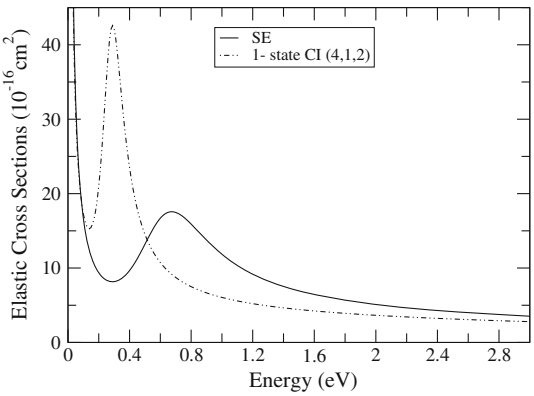

Figure 4. Shape resonance in SE and 1-state CI models in 1 $^1A_1$ scattering state.

cross-sections exhibit a threshold followed by a steep rise in cross-section and are significantly smaller than the ECS. This is due to smaller value of transition moment and higher target thresholds of excited states. The noticeable feature is that even though the ECS converged with respect to different active spaces (figure 1), the inelastic cross-sections showed considerable variation with respect to active space (4, 1, 2). The convergence however, improves as the active space became bigger.

2.2 *Resonance analysis*

The temporary trapping of an electron to form a short-lived state is known as resonance. The understanding of resonances and their decay behaviour is necessary in fields like aeronomy, lasers, radiation chemistry, physics [54] etc. At resonance, the electron gets trapped by centrifugal barrier and the attractive polarization of the molecule. This lead to a sudden rise in cross-section and π radians change in the eigenphase.

The L^2 configuration for the SE case is represented by $1a_1^2 2a_1^2 1b_2^2 3a_1^2 1b_1^1$. It captures the shape resonance in $^1A_1$ scattering symmetry. This resonance shifts towards the lower energy in 1-state CI model of (4, 1, 2) active space due to the inclusion of additional correlation effects. This effect is clearly visible in figure 4. Further, this resonance becomes the ground state of NH_2^- anion in 3-states CI model of (4, 1, 2) active space as well as in higher active spaces suggesting that the resonances are strongly influenced by correlation and polarization effects.

2.3 *Rate constants*

The rate constants for any given process is given by [55]

$$k(T_e) = \left(\frac{2}{m_e}\right)^{1/2} \int_0^\infty E^{1/2} Q(E) f_m(E, T_e) \mathrm{d}E, \quad (4)$$

where m_e is the mass of the electron, k_B is the Boltzmann's constant, T_e is the electron temperature, E is the energy of electron, $Q(E)$ is the relevant cross-section and $f_m(E, T_e)$ is the energy distribution function. At thermal equilibrium, the electron energy distribution is described by Maxwellian type and is a characteristic of gas temperature only. The rate constants for elastic and inelastic processes are extracted from the Born-corrected R-matrix cross-sections determined in 3-states CI model using the expression

$$k_i(T_e) = \left(\frac{8}{m_e \pi}\right)^{1/2} \left(\frac{1}{k_\mathrm{B} T_e}\right)^{3/2} \times \int_0^\infty E \sigma_i(E) \mathrm{e}^{-E/k_\mathrm{B} T_e} \mathrm{d}E. \quad (5)$$

For elastic cross-sections i is zero and for electron-excited inelastic cross-sections i is non-zero. The rate constants are studied up to 30,000 K and are plotted in figures 5 and 6. They are substantially smaller for inelastic processes due to their smaller cross-sections. The rate constant for X $^2B_1 \rightarrow 1\,^2B_2$ are multiplied by 100 in order to plot in figure 6 along with X $^2B_1 \rightarrow 1\,^2A_1$.

2.4 *Differential cross-section*

The DCS offers a stringent test for scattering calculations. They are needed to obtain momentum transfer and viscosity cross-sections and effective collision frequency. The DCS for a non-polar polyatomic molecule is given by

$$\frac{\mathrm{d}\sigma}{\mathrm{d}\Omega} = \sum_L A_L \; P_L(\cos\theta), \quad (6)$$

where A_L is the expansion coefficient and P_L is the Legendre function [55]. The summation over L converges

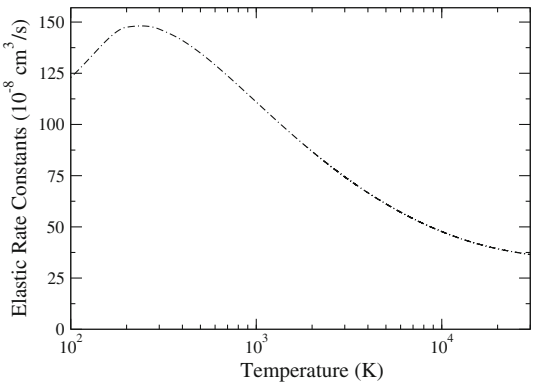

Figure 5. Elastic rate constants.

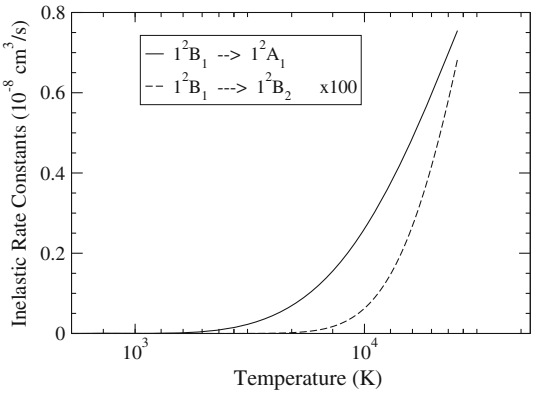

Figure 6. Inelastic rate constants for various excited states. The X $^2B_1 \rightarrow 1\,^2B_2$ values are multiplied by 100 times.

poorly for polar molecules thus giving diverging integral cross-sections in the forward direction. This problem is circumvented by using the closure formula [33]

$$\frac{\mathrm{d}\sigma}{\mathrm{d}\Omega}(J\tau \rightarrow J'\tau') = \frac{\mathrm{d}\sigma^B}{\mathrm{d}\Omega} + \sum_L (A_L - A_L^B)\, P_L(\cos\theta), \tag{7}$$

where $|J\tau\rangle$ and $|J'\tau'\rangle$ are the initial and final rotor states respectively, A_L^B and $\mathrm{d}\sigma^B/\mathrm{d}\Omega$ are the quantities calculated under Born approximation. The first term is the DCS for the rotating dipole in Born approximation. The second term represents the close coupling cross-sections while the third term is the contribution from higher partial waves and is dominated by the electron–dipole interaction. This term helps to obtain converged DCS. The rotationally summed elastic cross-sections can then be expressed as

$$\frac{\mathrm{d}\sigma^{\mathrm{summed}}}{\mathrm{d}\Omega} = \sum_{J'\,\tau'} \frac{\mathrm{d}\sigma}{\mathrm{d}\Omega}(J\tau \rightarrow J'\tau'). \tag{8}$$

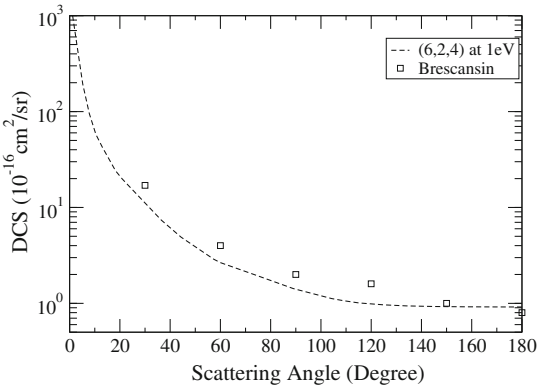

Figure 7. Rotationally summed DCS at 1 eV.

The summed DCS given by eq. (8) has contributions from the singlet and triplet states with appropriate statistical weights. The DCS is independent of initial rotational state of the target molecule and hence the rotational temperature as long as the scattering angle is not close to 0° [56].

The input to POLYDCS are basic molecular data, K-matrix elements generated in R-matrix calculations and the rotational constants of the molecule. The rotational constants $A = 0.0029430$ eV, $B = 0.0016046$ eV and $C = 0.0010384$ eV obtained are in excellent agreement with the reported values of Morino and Kawaguchi [26] and Burkholder *et al* [57]. A good convergence of rotational cross-sections is obtained by including J' up to 5. The rotationally summed DCS from $J = 0 \rightarrow J'(0-5)$ at different energies are shown in figures 7–11. The sharp rise in DCS at very small scattering angles is due to the strong polar nature of the target. The rotational energy levels corresponding to different values of J' are shown in table 4.

2.5 *Momentum-transfer cross-section*

The momentum-transfer cross-section (MTCS) is useful for solving the Boltzmann equation for the electron distribution function, diffusion parameters, molecular bremsstrahlung process etc. It indicates the amount of backward scattering. Unlike DCS, the MTCS does not exhibit singularity in forward direction due to the weighting factor $(1 - \cos\theta)$. The MTCS is obtained by integrating DCS over the scattering angle using the relation

$$Q^m = 2\pi \int_0^\pi \sin\theta(1 - \cos\theta)\frac{\mathrm{d}\sigma^{\mathrm{summed}}}{\mathrm{d}\theta}\mathrm{d}\theta. \tag{9}$$

The MTCS reported in figure 12 varies smoothly with energy and also compare well with the results of Brescansin *et al* [28].

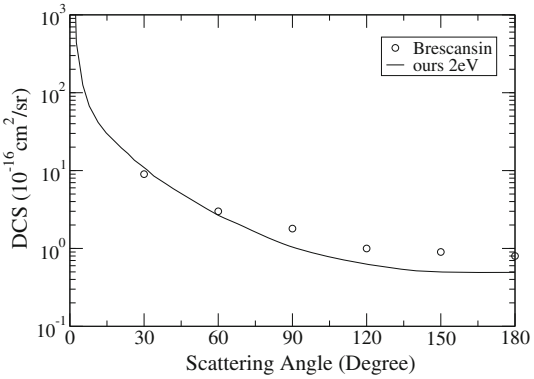

Figure 8. Rotationally summed DCS at 2 eV.

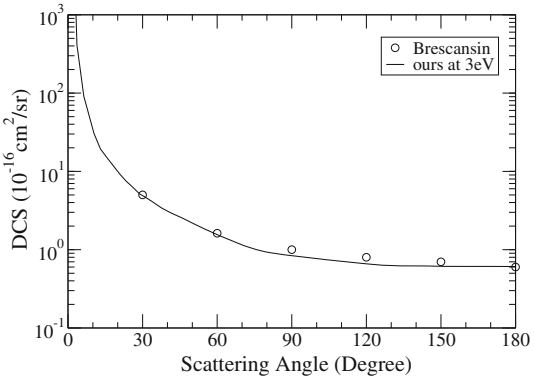

Figure 9. Rotationally summed DCS at 3 eV.

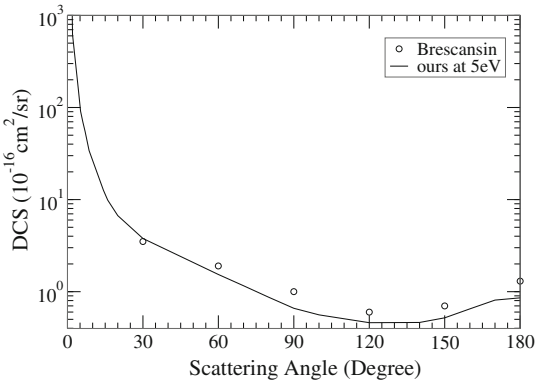

Figure 10. Rotationally summed DCS at 5 eV.

2.6 *Effective collision frequency*

The effective collision frequency is required for understanding plasma transport properties like electron mobility, electron diffusion coefficient etc. It is obtained by appropriately averaging MTCS over the energy distribution of electrons. In Maxwellian plasma, the effective electron–NH_2 collision frequencies $\langle \nu \rangle$ and $\bar{\nu}^{-1}$ can be obtained from $Q^m(v)$ using [58]

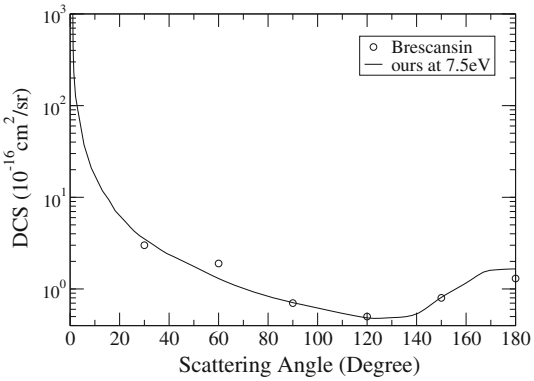

Figure 11. Rotationally summed DCS at 7.5 eV.

Table 4. The rotational energy levels of an asymmetric top NH_2 molecule.

J'	τ'	Energy (eV)
0	0	0.0
1	−1	0.00455
1	0	0.2659
1	1	0.2672
2	−2	0.0136
2	−1	0.2736
2	0	0.2777
2	1	1.0617
2	2	1.0617
3	−3	0.0277
3	−2	0.2853
3	−1	0.2933
3	0	1.0753
3	1	1.0753
3	2	2.3854
3	3	2.3854
4	−4	0.0454
4	−3	0.3008
4	−2	0.3142
4	−1	1.0935
4	0	1.0936
4	1	2.4036
4	2	2.4036
4	3	4.2376
4	4	4.2376
5	−5	0.0680
5	−4	0.3202
5	−3	0.3402
5	−2	1.1162
5	−1	1.1164
5	0	2.4263
5	1	2.4263
5	2	4.2604
5	3	4.2604
5	4	6.6184
5	5	6.6184

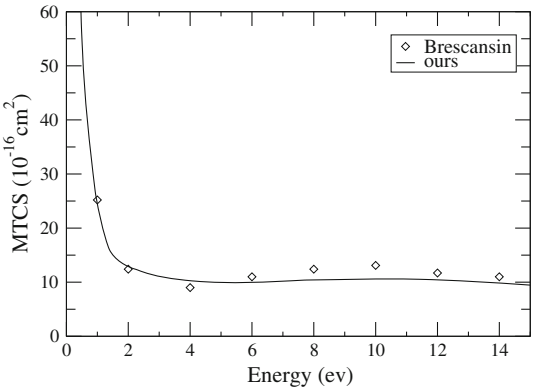

Figure 12. MTCS.

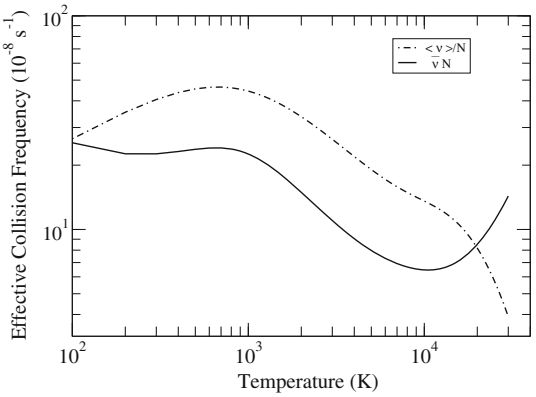

Figure 13. Effective collision frequency.

$$\langle \nu \rangle = \frac{8}{3\pi^{1/2}} N \left(\frac{m_e}{2k_B T_e} \right)^{5/2} \times \int_0^\infty v^5 Q^m(v) e^{-m_e v^2/2k_B T_e} dv \quad (10)$$

and

$$\bar{\nu}^{-1} = \frac{8}{3\pi^{1/2} N} \left(\frac{m_e}{2k_B T_e} \right)^{5/2} \times \int_0^\infty \frac{v^3}{Q^m(v)} e^{-m_e v^2/2k_B T_e} dv. \quad (11)$$

Here, N is the number density of gas molecules, m_e is the electron mass, k_B is the Boltzmann factor, T_e is electron temperature, v is the velocity of the electron and $Q^m(v)$ is the velocity-dependent MTCS. The variation of $\langle \nu \rangle$ and $\bar{\nu}^{-1}$ with temperature up to 30,000 K is shown in figure 13.

2.7 *Molecular bremsstrahlung radiation cross-section*

The study of emission of bremsstrahlung radiation during the collision of electrons is one of the focus

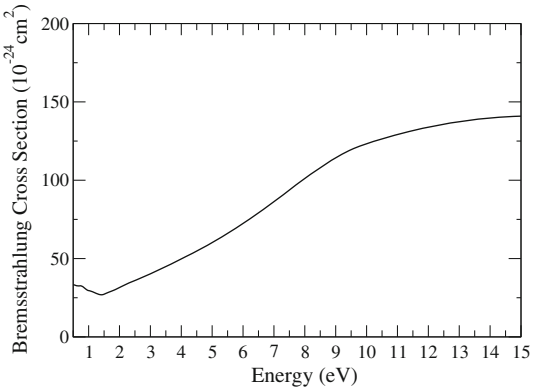

Figure 14. Molecular bremsstrahlung cross-sections for soft photons in low collision energy limit.

of quantum electrodynamics. The free–free molecular cross-section due to electron collision Q_{ff} is expressed as [59]

$$Q_{ff}(E, h\nu) = \frac{4\alpha^3}{3R\pi} \left(1 - \frac{h\nu}{2E} \right) \left(1 - \frac{h\nu}{E} \right)^{1/2} E Q^m(E), \quad (12)$$

where α is the fine-structure constant, R is the Rydberg energy and $Q^m(E)$ is the energy-dependent MTCS. Considering only the low-energy electrons and soft photons ($h\nu \ll E$), eq. (12) may be rewritten as

$$Q_{ff}(E, h\nu) = \beta E Q^m(E), \quad (13)$$

where $\beta = 1.211 * 10^{-8}$. The low kinetic energy electrons in the range of 1–10 eV and photons of GHz energy range validates the above approximation. At GHz range of photon energy, plasma dispersion effects become negligible. Equation (13) can be regarded as upper limit to the free–free molecular cross-section. The MTCS can also be used to calculate emissivity, absorption coefficient and source function of low-energy photons. These parameters are important in plasma and space physics while studying microwave emission due to molecular bremsstrahlung [60]. The bremsstrahlung cross-sections for electron energies are plotted in figure 14.

2.8 *Ionization cross-section*

The BEB ionization cross-sections in the non-relativistic limit [61] as a function of incident electron energy E is given by

$$\sigma_i(t) = \frac{S}{t + (u+1)} \left[\frac{1}{2} \left(1 - \frac{1}{t^2} \right) \ln t + \left[\left(1 - \frac{1}{t} \right) - \frac{\ln t}{t+1} \right] \right], \quad (14)$$

Table 5. Molecular orbitals, binding energy and average kinetic energy (in eV) and occupancy number of NH_2.

Molecular orbital	$\|B\|$	U	N
$1a_1$	−423.94	601.9803	2
$2a_1$	−29.95	50.3260	2
$1b_2$	−17.22	43.6839	2
$3a_1$	−13.07	46.9104	2
$1b_1$	−6.82	35.7381	1

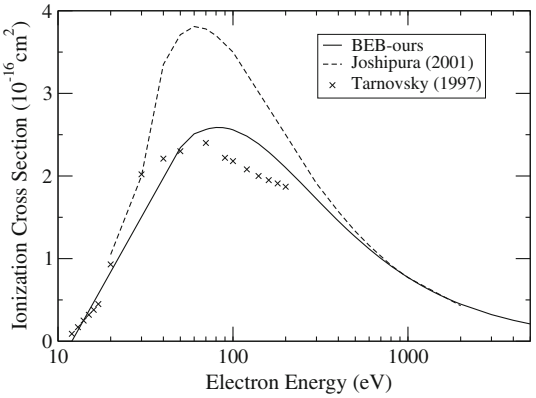

Figure 15. Non-relativistic electron impact BEB ionization cross-section.

where $t = E/B$, $u = U/B$ are the normalized energies, $S = 4\pi a_0^2 N(R/B)^2$, R is the Rydberg energy, a_0 is Bohr's radius, B is the binding energy of the orbital, U is the orbital kinetic energy and N is the orbital occupation number. The total ionization cross-section is obtained by summing cross-sections of individual molecular orbitals for $E > B$. This model is known to behave correctly up to 20 keV [62].

The molecular orbital data are given in table 5. The BEB ionization cross-sections shown in figure 15 are from threshold. Joshipura *et al* [29] obtained upper bounds to the total ionization cross-sections using complex optical potential method. They added the charge density distribution of constituent atoms to generate charge distribution density for molecules. The ionization cross-sections were extracted from inelastic cross-sections while Deutsch *et al* [31] used additive rule to calculate lower bounds of electron impact ionization cross-sections of molecules and radicals. Our value $2.67 * 10^{-16}$ cm^2 of BEB ionization cross-section at 70 eV lies between the upper bound value $3.78 * 10^{-16}$ cm^2 and lower bound value $2.40 * 10^{-16}$ cm^2. It also agrees with the summed partial ionization cross-section value $2.40 * 10^{-16}$ cm^2 obtained by Tarnovsky *et al* [30] within experimental uncertainties. The electron impact BEB ionization cross-sections show trend and shape similar to theirs, thus validating the cross-section data.

3. Conclusion

This paper reports electron-scattering calculations using the R-matrix close-coupling method together with an application of BEB model for NH_2 molecule. There is a good quantitative agreement of our results with that of Brescansin *et al*. The overall shape of the angular distribution is also very similar to the sampled data. We have also reported electron impact inelastic cross-sections along with rate coefficients for some low-lying electronic states of NH_2. This paper addresses the key issue of convergence of cross-sections with respect to the active spaces. The shape resonance detected in SE and 1-state CI model of (4, 1, 2) vanishes on inclusion of excited states in trial wave function or by including greater correlation effects, thus giving rise to bound state NH_2^-. Both inelastic cross-sections and resonance formation are found to be sensitive to the correlation and polarization effects. The bremsstrahlung phenomenon has applications in space and atmospheric physics and is an integral part in the study of quantum electrodynamics. This theoretical study assumes significance as it fulfills the lack of electron radical collision cross-sections which are difficult to measure experimentally. The theoretical data generated here would be immensely useful in various branches of applied physics.

Acknowledgements

The authors are grateful to Prof. Jonathan Tennyson for his guidance and encouragement provided in carrying out this work.

References

[1] Z B Fassi, *The chemistry of free radicals: N-Centered radicals* (Wiley, Hoboken, 1998).
[2] N J Mason, J M Gingell, N C Jones and L Kaminski, *Philos. Trans. R. Soc. London A* **357**, 1175 (1999)
[3] N L Aleksandrov, S V Kindysheva, I N Kosarev, S M Starikovskaia and A Y Starikovskii, *Proc. Combust. Inst.* **32**, 205 (2009)
[4] S M Starikovskaia, A Y Starikovskii and D V Zatsepin, *Combust. Theory Model.* **5**, 97 (2001)
[5] C Duynslaeger, F Contino, J Vandooren and H Jeanmart, *Combust. Flame* **159**, 2799 (2012)
[6] V Vuitton, R V Yelle and V G Anicich, *Astrophys. J.* **647**, L175 (2006)
[7] D F Davidson, K Kohse-Höinghaus, A Y Chang and R K Hanson, *Int. J. Chem. Kinet.* **22**, 513 (1990)
[8] O Skreiberg, P Kilpinen and P Glarborg, *Combust. Flame* **136**, 501 (2004)
[9] A A Konnov and J de Ruyck, *Combust. Sci. Technol.* **124**, 106 (2001)

[10] C I Butoi, M L Steen, J R D Peers and E R Fisher, *J. Phys. Chem. B* **105**, 5957 (2001)
[11] I Rahinov, N Ditzian, A Goldman and S Cheskis, *Appl. Phys. B* **77**, 541 (2003)
[12] P J van den Oever, J H van Helden, J L van Hemmen, R Engeln, D C Schram, M C M van de Sanden and W M M Kessels, *J. Appl. Phys.* **100**, 093303 (2006)
[13] W C Gardner Jr, *Gas-phase combustion chemistry* (Springer, New York, 1999)
[14] J A Miller and C T Bowman, *Prog. Energy Combust.* **15**, 287 (1989)
[15] T Owen, *Nature* **438**, 756 (2005)
[16] C M Persson *et al*, *Astron. Astrophys. A* **543**, 145 (2012)
[17] H Kawakita and M Mumma, *Astrophys. J.* **727**(**2**), 91 (2011)
[18] F Holzmeier, M Lang, I Fischer, P Hemberger, G A Garcia, X Tangc and J-C Loisond, *Phys. Chem. Chem. Phys.* **17**, 19507 (2015)
[19] F J Dentener and P J J Crutzen, *Atmos. Chem.* **19**, 331 (1994)
[20] H S P Muller, H Klein, S P Belov, G Winnewisser, I Morino, K M T Yamada and S Saito, *J. Mol. Spectrosc.* **195**, 177 (1999)
[21] R Gendriesch, F Lewen, G Winnewisser and H S P Muller, *J. Mol. Struct*. **293**, 599 (2001)
[22] R Vetter, L Zulicke, A Koch, E F van Dishoeck and S D Peyerimhoff, *J. Chem. Phys.* **104**(**14**), 5558 (1996)
[23] P Jensen, W P Kraemer and P R Bunker, *Mol. Phys.* **101**(**4–5**), 613 (2003)
[24] P D Rajendra and P Chandra, *J. Chem. Phys.* **114**(**17**), 7450 (2001)
[25] Y Yamaguchi, B C Hoffman, J C Stephens and H F Schaefer III, *J. Phys. Chem. A* **103**, 7701 (1999)
[26] I Morino and K Kawaguchi, *J. Mol. Spectrosc.* **182**, 428 (1997)
[27] R P Saxon, B H Lengsfield III and B Liu, *J. Chem. Phys.* **78**(**1**), 312 (1983)
[28] L M Brescansin, M T Lee and L E Machado, *Int. J. Quantum Chem.* **108**, 2312 (2008)
[29] K N Joshipura, M Vinodkumar and U M Patel, *J. Phys. B* **34**, 509 (2001)
[30] V Tarnovsky, H Deutsch and K Becker, *Int. J. Mass Spectrosc. Ion Process.* **167**/**168**, 69 (1997)
[31] H Deutsch, K Becker and T D Mark, *Int. J. Mass Spectrosc. Ion Process.* **167**/**168**, 503 (1997)
[32] J M Carr, P G Galiatsatos, J D Gorfinkiel, A G Harvey, M A Lysaght, D Madden, Z Masin, M Plummer, J Tennyson and H N Varambhia, *Eur. Phys. J. D* **66**, 58 (2012)
[33] N Sanna and F A Gianturco, *Comput. Phys. Commun.* **114**, 142 (1998)
[34] E P Wigner, *Phys. Rev.* **70**, 15 (1946)
[35] A M Lane and R G Thomas, *Rev. Mod. Phys.* **30**, 257 (1958)
[36] M Le Dourneuf, B I Schneider and P G Burke, *J. Phys. B* **12**, L365 (1979)
[37] P G Burke, *R-matrix theory of atomic collisions: Application to atomic, molecular and optical processes* (Springer, Berlin, 2011)
[38] J Tennyson, *Phys. Rep.* **491**, 29 (2010)
[39] L A Morgan, C J Gillan, J Tennyson and X Chen, *J. Phys. B: At. Mol. Opt. Phys.* **30**, 4087 (1997)
[40] B M Nestmann, K Pfingst and S D Peyerimhoff, *J. Phys. B: At. Mol. Opt. Phys.* **27**, 2297 (1994)
[41] T H Dunning and P J Hay, *Methods of electronic structure theory* edited by H F Schaefer (Plenum, New York, 1977) Vol. 2
[42] K L Baluja, P G Burke and L A Morgan, *Comput. Phys. Commun.* **27**, 299 (1982)
[43] L A Morgan, *Comput. Phys. Commun.* **31**, 419 (1984)
[44] B N Plakhutin, E V Gorelik and B N Breslavskaya, *J. Chem. Phys.* **125**, 204110 (2006)
[45] J M Brown, S W Chalkley and F D Wayne, *Mol. Phys.* **38**, 1521 (1979)
[46] M Kallay and J Gauss, *J. Chem. Phys.* **121**(**19**), 9257 (2004)
[47] J B Halpern, G Hancock, M Lenzi and K H Welge, *J. Chem. Phys.* **63**, 4808 (1975)
[48] S D Peyerimhoff and R J Buenker, *Can. J. Chem.* **57**, 3182 (1979)
[49] http://cccbdb.nist.gov/
[50] A Faure, J D Gorfinkiel, L A Morgan and J Tennyson, *Comput. Phys. Commun.* **144**, 224 (2002)
[51] K L Baluja, N J Mason, L A Morgan and J Tennyson, *J. Phys. B: At. Mol. Opt. Phys.* **34**, 4041 (2001)
[52] K L Baluja, N J Mason, L A Morgan and J Tennyson, *J. Phys. B: At. Mol. Opt. Phys.* **34**, 2807 (2001)
[53] D W Norcross and N T Padial, *Phys. Rev. A* **25**, 226 (1982)
[54] J B Hasted and D Mathur, Electron–molecule resonances, in: *Electron–molecule interactions and their applications* edited by L G Christophorou (Academic Press, New York, 1984) Vol. 1, p. 403
[55] F A Gianturco and A Jain, *Phys. Rep.* **143**, 347 (1986)
[56] Y Okamoto, K Onda and Y Itikawa, *J. Phys. B: At. Mol. Opt. Phys.* **26**, 745 (1993)
[57] J B Burkholder, C J Howard and A R W McKellar, *J. Mol. Spectrosc.* **127**, 415 (1988)
[58] Y Itikawa, *Phys. Fluids* **16**, 831 (1973)
[59] I Al Samarai, O Deligny, D Lebrun, A Letessier-Selvon and F Salamida, *Astropart. Phys.* **67**, 26 (2015)
[60] P W Gorham, N G Lehtinen, G S Varner, J J Beatty, A Connolly, P Chen, M E Conde, W Gai, C Hast, C L Hebert, C Miki, R Konecny, J Kowalski, J Ng, J G Power, K Reil, L Ruckman, D Saltzberg, B T Stokes and D Walz, *Phys. Rev. D* **78**, 032007 (2008)
[61] Y K Kim, W Hwang, N M Weinberger, M A Ali and M E Rudd, *J. Chem. Phys.* **106**, 1026 (1997)
[62] J P Santos, F Parente and Y K Kim, *J. Phys. B: At. Mol. Opt. Phys.* **36**(**21**), 4211 (2003)